Steady-State Cornering Equilibria and Stabilization for a Vehicle During Extreme Operating Conditions.

Efstathios Velenis[1], Emilio Frazzoli[2] and Panagiotis Tsiotras[3]

Abstract

In this work we study steady-state cornering conditions for a single-track vehicle model without imposing restrictive (i.e., linearized) conditions on the tire slip. For each steady-state cornering condition we calculate the corresponding tire friction forces at the front and rear tires, as well as the required front steering angle and front and rear wheel slip ratios, to maintain constant velocity, turning rate and vehicle sideslip angle. Inspired by recent progress in the understanding of advanced driving techniques, we design a sliding-mode control scheme stabilizing steady-state cornering conditions, using only longitudinal control inputs, i.e, accelerating/braking torques applied at the front and/or rear wheels. The effectiveness of the control scheme is demonstrated by implementing it in a variety of simulation scenarios, including cornering at extreme sideslip angles, similar to the operating regimes encountered in competitive race driving. Simulation results are presented using both the baseline model, and an increased-fidelity model taking into account the suspension dynamics.

Keywords: Vehicle dynamics, technical driving, drift, steady-state cornering, nonlinear tire characteristics, stabilization, sliding mode control.

1 Introduction

The introduction of vehicle stability systems has had a significant impact on passenger vehicle safety. Several statistics show that these systems have considerably reduced road traffic accidents [Dang, 2004]. There is a variety of results in the literature towards enhancing the performance of passenger vehicle stability systems. Stability control is usually implemented via differential braking (independent braking control on all four wheels) [T. van Zanten et al., 2000], active steering [Ackermann, 1997], [Yoshimoto et al., 1999], active-differential [Ikushima and Sawase, 1995], [Piyabongkarn et al., 2007] and, more recently, via integrated chassis control [Hac and Bodie, 2002], [Trachtler, 2004], [Wei et al., 2006]. The latter incorporate and co-ordinate active chassis systems including differential braking, traction control, active steering and active suspension systems. Alternative means of power transmission for electric and hybrid vehicles have also allowed the development of vehicle stability systems based on independent wheel torque control [Tahami et al., 2003], [Kim et al., 2008]. The common objective of all of the above systems is to restrict the operation of the vehicle, such that the tires operate within the linear region of the wheel slip-tire friction characteristic, and to match the vehicle's response to one of a simple vehicle model in steady-state cornering [Gillespie,

[1]School of Engineering and Design, Brunel University, Uxbridge, Middlesex, UB8-3PH, UK Email: efstathios.velenis@brunel.ac.uk, Corresponding author

[2]Department of Aeronautics and Astronautics, Massachusetts Institute of Technology, Cambridge, MA 02139, USA, Email: frazzoli@mit.edu

[3]Daniel Guggenheim School of Aerospace Engineering, Georgia Institute of Technology, Atlanta, GA 30332-0150, USA, Email: tsiotras@gatech.edu

1992]. In this way, the average driver can maintain control of the vehicle during an emergency. It is worth pointing out that, while traditionally stability analysis and control considered solely the lateral dynamics of the vehicle, there have been recent results incorporating longitudinal and lateral dynamics and the coupling of tire forces in the longitudinal/lateral directions [Wei et al., 2006], [Yi and Tseng, 2009].

Accident avoidance during an emergency may require taking advantage of the full handling capacity of the vehicle, and the employment of expert driving skills, rather than restricting the response of the vehicle. It is envisioned that a new generation of active safety systems will take advantage of the increased situational awareness of modern and future vehicles, as demonstrated during the 2005 DARPA Grand Challenge and the 2007 DARPA Urban Challenge autonomous vehicle competitions, and use expert driver techniques to actively maneuver vehicles away from accidents. With this vision in mind, a mathematical analysis of expert driving techniques was initiated in [Velenis et al., 2007a], [Velenis et al., 2007b], [Velenis et al., 2008a] and [Velenis et al., 2008b]. The driving techniques investigated in these references were those used by rally drivers, which clearly involve operation of the vehicle outside the stable operation envelope enforced by the current stability systems. Data collected during execution of different rally driving techniques by an expert driver in [Velenis et al., 2007b] and [Velenis et al., 2008b] show operation of the vehicle at high sideslip angles, suggesting that the tires operate well inside the nonlinear region. These expert driving techniques were reproduced using nonlinear programming optimization [Velenis et al., 2007a], [Velenis et al., 2007b], [Velenis et al., 2008a] and [Velenis et al., 2008b]. It was shown that cornering at high sideslip angles may be necessary for time-optimal cornering with limited preview of the road. Furthermore, expert drivers' empirical guidelines on controlling the vehicle under such extreme operating conditions, via throttle/brake control and longitudinal load transfer, were validated. The analysis in [Velenis et al., 2007a], [Velenis et al., 2007b], [Velenis et al., 2008a] and [Velenis et al., 2008b] provided a significant understanding of the dominant effects during execution of expert driving techniques, but the open-loop approach of the optimization is not implementable in the presence of uncertainties.

A study of the stability of vehicle cornering equilibria with the tires operating at their full range (including linear and nonlinear range) and the design of a stabilizing front wheel steering controller appear in [Ono et al., 1998]. The authors of this work used a single-track vehicle model and assumed pure cornering conditions, that is, absence of longitudinal forces (tractive or braking) at the wheels. A phase-plane analysis of the cornering equilibria in this work was followed by the design of a linear robust stabilizing steering controller. The stability analysis of cornering equilibria considering nonlinear tire characteristics and using phase-plane techniques is also discussed in [Yi and Tseng, 2009]. In the latter a combined motion tire friction model is used to characterize the coupling of tire forces in the longitudinal and lateral directions. High sideslip angle (drifting) steady-state cornering conditions were examined in [Abdulrahim, 2006] using the lateral dynamics of a four wheel vehicle model, neglecting the equilibrium of forces in the longitudinal direction. A combined traction/cornering tire friction model was incorporated and under the assumption of rear-wheel-drive (RWD) transmission the steady-state steering angle and rear wheel slip ratio were derived for a given pair of steady-state sideslip angle and yaw rate. Steady-state drifting or power-slide using a four wheel vehicle model with RWD transmission, incorporating longitudinal and lateral dynamics, load transfer effects and a combined motion tire friction model, have been discussed in [Edelmann et al., 2008]. The set of steady-state equations were solved numerically and stability of the equilibria was studied using a root locus method. A simple single-track model of an RWD vehicle incorporating longitudinal and lateral vehicle dynamics and a simplified combined motion tire friction model were used in [Hindiyeh and Gerdes, 2009] for a stability analysis and classification of cornering equilibria including drifting conditions. Using a simplified tire

friction model the authors in [Hindiyeh and Gerdes, 2009] neglected the wheel speed dynamics and considered the rear wheel longitudinal force as a control input. Neglecting load transfer effects and wheel rotational dynamics, the vehicle model in [Hindiyeh and Gerdes, 2009] is of low order and more suitable for control design compared, for instance, to the high fidelity model of [Edelmann et al., 2008].

The existence of steady-state cornering conditions with excessive vehicle sideslip was also demonstrated in [Frazzoli, 2008]. In this reference the author derived explicit steady-state cornering conditions for a single-track vehicle model using a wheel slip based combined motion tire friction model, and considering longitudinal load transfer effects, which play a key role in the execution of expert driving techniques as discussed in [Velenis et al., 2007a], [Velenis et al., 2007b], [Velenis et al., 2008a] and [Velenis et al., 2008b]. The simplifying assumption of a free rolling rear wheel in [Frazzoli, 2008], which suggests a front-wheel-drive configuration, allowed for considerable decoupling of the steady-state equations and efficient calculation of the equilibria. Building on the approach of [Frazzoli, 2008], in this work we allow for the combined cornering and traction/braking forces to develop on both front and rear tires, assuming independent front and rear longitudinal slip inputs, and derive cornering equilibria achievable by different transmission configurations (front-, rear-, all-wheel-drive). The vehicle model is enriched with wheel speed dynamics and load transfer effects, which results in a higher order model than the one in [Hindiyeh and Gerdes, 2009], remaining, however, suitable for control design. In particular, we design a control scheme using independent wheel front and rear torque inputs to stabilize the vehicle with respect to steady-states cornering conditions including drifting. In the proposed control scheme the steering angle is fixed at its steady-state value, and stabilization is achieved purely by regulation of tractive/braking forces in analogy to previously studied expert driving techniques [Velenis et al., 2007a], [Velenis et al., 2007b], [Velenis et al., 2008a] and [Velenis et al., 2008b]. We envision the ability to control the vehicle in a wide range of steady-state cornering conditions, including large vehicle sideslip angles, as an enabling technology towards the development of full-envelope vehicle control technologies, emulating the skills of expert drivers, e.g., for accident avoidance or high-performance driving. For example, a library of motion primitives consisting of a collection of pre-computed steady-state trajectories and controlled transitions can be used to construct "aggressive" trajectories on the fly [Frazzoli et al., 2002], [Frazzoli et al., 2005].

In the following, we first introduce a single-track model with nonlinear tire characteristics, taking into consideration the normal load transfer from front to rear wheels during forward acceleration. Steady-state cornering is defined as cornering along a path of constant curvature, with constant speed and sideslip angle. For a given triplet of corner curvature, vehicle speed and sideslip angle, we calculate the necessary front and rear wheel longitudinal slip quantities (slip ratios), and front wheel steering angle, necessary to maintain the steady-state cornering condition. Steady-state wheel speeds and the corresponding torques at the front and the rear axles are then calculated using the associated wheel speed dynamics. A control scheme is presented, consisting of a linear quadratic regulator, which produces the necessary front and rear longitudinal slip quantities to stabilize the vehicle to the desired triplet of steady-state speed, sideslip angle and yaw rate, and a sliding-mode controller, which uses front and rear wheel torques to drive the front and rear longitudinal slips to the values dictated by the LQR. A vehicle model of increased fidelity, namely a single-track model with suspension dynamics, is used to demonstrate the efficiency of the controller.

2 Vehicle Model

In this section we introduce a single-track vehicle model with nonlinear tire characteristics. We employ a static map to calculate the normal load transfer from front to rear wheels, and

vice-versa, arising from the longitudinal acceleration of the vehicle. This model maintains a satisfactory level of fidelity for reproducing the dominant vehicle dynamic effects during extreme operating conditions, such as those encountered in rally driving [Velenis et al., 2007a], [Velenis et al., 2008a], [Velenis et al., 2008b].

2.1 Equations of Motion of the Single-Track Model

The equations of motion of the single-track model (Fig. 1) may be expressed in a body-fixed frame with the origin at the vehicle's center of gravity (C.G.) as follows:

$$m\left(\dot{V}_x - V_y\dot{\psi}\right) = f_{Fx}\cos\delta - f_{Fy}\sin\delta + f_{Rx} \quad (1)$$

$$m\left(\dot{V}_y + V_x\dot{\psi}\right) = f_{Fx}\sin\delta + f_{Fy}\cos\delta + f_{Ry} \quad (2)$$

$$I_z\ddot{\psi} = (f_{Fy}\cos\delta + f_{Fx}\sin\delta)\,\ell_F - f_{Ry}\ell_R, \quad (3)$$

where

$$V_x = V\cos\beta, \qquad V_y = V\sin\beta.$$

In the above equations m is the vehicle's mass, I_z is the moment of inertia of the vehicle about the vertical axis, V_x and V_y are the body-frame components of the vehicle velocity V, ψ is the yaw angle of the vehicle, and δ is the steering angle of the front wheel. By f_{ij} $(i = F, R$ and $j = x, y)$ we denote the longitudinal and lateral friction forces at the front and rear wheels, respectively.

The vehicle slip angle is given by

$$\beta = \text{atan}\left(\frac{\dot{y}}{\dot{x}}\right) - \psi = \text{atan}\left(\frac{V_y}{V_x}\right)$$

where $\dot{x}$ and $\dot{y}$ are the inertial frame components of the vehicle speed.

2.2 Tire Forces

By tire slip we refer to the non-dimensional relative velocity of the tire with respect to the road. In [Bakker et al., 1987] the practical tire slip quantities, namely the practical longitudinal slip κ_i and the slip angle α_i $(i = F, R)$, are defined as follows:

$$\kappa_i = \frac{\omega_i r_i - V_{ix}}{V_{ix}}, \qquad \tan\alpha_i = \frac{V_{iy}}{V_{ix}},$$

where the index $i = F, R$ denotes the front and rear axle of the single-track model respectively, ω_i is the angular rate of the wheel, r_i is the wheel radius, and V_{ij}, $(i = F, R,\ i = x, y)$ are the tire frame components of the vehicle velocity vector at the front and rear wheels.

The theoretical slip quantities [Bakker et al., 1987] are defined as:

$$s_{ix} = \frac{V_{ix} - \omega_i r_i}{\omega_i r_i} = -\frac{\kappa_i}{1+\kappa_i}, \qquad s_{iy} = \frac{V_{iy}}{\omega_i r_i} = \frac{\tan\alpha_i}{1+\kappa_i}. \quad (4)$$

We notice that

$$s_{iy} = (1 + s_{ix})\tan\alpha_i.$$

The overall, or total, slip at each tire is defined by

$$s_i = \sqrt{s_{ix}^2 + s_{iy}^2}.$$

The vehicle velocity components at the front and rear wheels of the single-track model along each wheel's longitudinal and lateral axes are given by:

$$V_{Fx} = V\,\cos(\beta-\delta) + \dot{\psi}\,\ell_f\,\sin\delta, \qquad V_{Fy} = V\,\sin(\beta-\delta) + \dot{\psi}\,\ell_f\,\cos\delta$$
$$V_{Rx} = V\,\cos(\beta), \qquad V_{Ry} = V\,\sin(\beta) - \dot{\psi}\,\ell_R.$$

Assuming linear dependence of the tire friction forces on the tire normal force we obtain

$$\mu_i = f_i/f_{iz}, \quad \mu_{ij} = f_{ij}/f_{iz}, \qquad i = F,R, \quad j = x,y, \tag{5}$$

where $f_i = \sqrt{f_{ix}^2 + f_{iy}^2}$ is the total friction force at each tire, μ_i is the total friction coefficient at each tire, μ_{ij} are the longitudinal and lateral friction coefficients at each tire, and f_{iz} are the normal loads at the front and rear tires.

We calculate the total friction coefficient using Pacejka's "magic formula" (MF) [Bakker et al., 1987] as follows:

$$\mu_i(s_i) = \mathrm{MF}(s_i) = D\sin(C\mathrm{atan}(Bs_i)).$$

Assuming symmetric tire characteristics with respect to the longitudinal and lateral directions, the total friction force for each tire lies within the so-called friction circle. In this case, the longitudinal and lateral tire friction components are given by:

$$\mu_{ij} = -\frac{s_{ij}}{s_i}\mu(s_i). \tag{6}$$

Neglecting suspension dynamics, the equilibrium of forces in the vertical direction and the equilibrium of moments about the body-y axis are used to find front and rear axle normal loads:

$$0 = f_{Fz} + f_{Rz} - mg, \tag{7}$$
$$0 = h\,(f_{Fx}\cos\delta - f_{Fy}\sin\delta + f_{Rx}) + f_{Fz}\ell_F - f_{Rz}\ell_R, \tag{8}$$

where h is the height of the C.G. from the road surface. Assuming linear dependence of the tire friction forces on the tire normal load (5), equations (7), (8) result in the following expressions for the front and rear wheel normal loads:

$$f_{Fz} = \frac{\ell_R mg - hmg\mu_{Rx}}{L + h\,(\mu_{Fx}\cos\delta - \mu_{Fy}\sin\delta - \mu_{Rx})}, \tag{9}$$
$$f_{Rz} = mg - f_{Fz}. \tag{10}$$

3 Steady-State Cornering Conditions

In this section we derive steady-state cornering conditions for the vehicle model of the previous section. For a given corner curvature, vehicle speed and sideslip angle, we calculate the corresponding tire friction forces of the front and rear wheels.

Steady-state cornering is characterized by a trajectory of constant radius R, negotiated at a constant speed V, and constant yaw rate and slip angle:

$$R = R^{\mathrm{ss}} = \text{const.}, \qquad V = V^{\mathrm{ss}} = \text{const.}, \qquad \dot{\psi} = \dot{\psi}^{\mathrm{ss}} = \frac{V^{\mathrm{ss}}}{R^{\mathrm{ss}}}, \qquad \beta = \beta^{\mathrm{ss}} = \text{const.}$$

Under steady-state cornering conditions, equations (1), (2), (3), (7) and (8) are summarized below:

$$-\frac{m(V^{\rm ss})^2}{R^{\rm ss}}\sin\beta^{\rm ss} = f_{Fx}^{\rm ss}\cos\delta^{\rm ss} - f_{Fy}^{\rm ss}\sin\delta^{\rm ss} + f_{Rx}^{\rm ss} \quad (11)$$

$$\frac{m(V^{\rm ss})^2}{R^{\rm ss}}\cos\beta^{\rm ss} = f_{Fx}^{\rm ss}\sin\delta^{\rm ss} + f_{Fy}^{\rm ss}\cos\delta^{\rm ss} + f_{Ry}^{\rm ss} \quad (12)$$

$$0 = \left(f_{Fx}^{\rm ss}\sin\delta^{\rm ss} + f_{Fy}^{\rm ss}\cos\delta^{\rm ss}\right)\ell_F - f_{Ry}^{\rm ss}\ell_R \quad (13)$$

$$0 = f_{Fz}^{\rm ss} + f_{Rz}^{\rm ss} - mg \quad (14)$$

$$0 = h\left(f_{Fx}^{\rm ss}\cos\delta^{\rm ss} - f_{Fy}^{\rm ss}\sin\delta^{\rm ss} + f_{Rx}^{\rm ss}\right) + f_{Fz}^{\rm ss}\ell_F - f_{Rz}^{\rm ss}\ell_R. \quad (15)$$

In the following we derive the conditions that the rear and front wheel slip quantities s_{ij} $(i = F, R,\ j = x, y)$ and corresponding wheel forces f_{ij} need to satisfy in order for the vehicle to maintain a steady-state triplet $(R^{\rm ss}, V^{\rm ss}, \beta^{\rm ss})$. Constraints with regards to the vehicle's transmission type (front-, rear- or all-wheel-drive) are neglected for the time being to simplify the calculations, and we allow for both tractive and braking forces to develop on both front and rear wheels assuming independently driven wheels, as in [Kim et al., 2008].

3.1 Rear Axle Steady-State Equations

Equations (12) and (13) can be solved for f_{Ry} as a function of $V^{\rm ss}$, $R^{\rm ss}$ and $\beta^{\rm ss}$, resulting in

$$f_{Ry}^{\rm ss} = \frac{m(V^{\rm ss})^2}{R^{\rm ss}}\cos\beta^{\rm ss}\frac{\ell_F}{\ell_F+\ell_R}.$$

Equations (11), (14) and (15) lead to the following expressions for the front and rear axle normal loads as functions of $V^{\rm ss}$, $R^{\rm ss}$ and $\beta^{\rm ss}$:

$$f_{Rz}^{\rm ss} = \frac{mg\ell_F - mh(V^{\rm ss})^2\sin\beta^{\rm ss}/R^{\rm ss}}{\ell_F+\ell_R}, \quad (16)$$

$$f_{Fz}^{\rm ss} = \frac{mg\ell_R + mh(V^{\rm ss})^2\sin\beta^{\rm ss}/R^{\rm ss}}{\ell_F+\ell_R}. \quad (17)$$

Hence, given $V^{\rm ss}$, $R^{\rm ss}$ and $\beta^{\rm ss}$ we can compute the steady-state $\mu_{Ry}^{\rm ss}$ from

$$\mu_{Ry}^{\rm ss} = \frac{f_{Ry}^{\rm ss}}{f_{Rz}^{\rm ss}},$$

as well as $\tan(\alpha_R^{\rm ss})$, from

$$\tan(\alpha_R^{\rm ss}) = \frac{V^{\rm ss}\sin\beta^{\rm ss} - V^{\rm ss}\ell_R/R^{\rm ss}}{V^{\rm ss}\cos\beta^{\rm ss}}.$$

Pacejka's Magic formula and the slip definitions result in the following three equations with three unknowns, namely $s_R^{\rm ss}$, $s_{Rx}^{\rm ss}$ and $s_{Ry}^{\rm ss}$:

$$\tan(\alpha_R^{\rm ss}) = \frac{s_{Ry}^{\rm ss}}{1+s_{Rx}^{\rm ss}} \quad (18)$$

$$s_R^{\rm ss} = \sqrt{(s_{Rx}^{\rm ss})^2 + (s_{Ry}^{\rm ss})^2} \quad (19)$$

$$\mu_{Ry}^{\rm ss} = -\frac{s_{Ry}^{\rm ss}}{s_R^{\rm ss}}{\rm MF}(s_R^{\rm ss}) \quad (20)$$

Solving equations (18), (19) and (20) for the rear tire slip quantities, finally leads to the computation of the longitudinal friction force at the rear wheel:

$$\mu_R^{\rm ss} = {\rm MF}(s_R^{\rm ss}), \quad \mu_{Rx}^{\rm ss} = -\frac{s_{Rx}^{\rm ss}}{s_R^{\rm ss}}\mu_R^{\rm ss}, \quad f_{Rx}^{\rm ss} = \mu_{Rx}^{\rm ss} f_{Rz}^{\rm ss}.$$

3.2 Front Axle Steady-State Equations

Equations (11) and (12) result in the following calculation of the total front axle friction force, as a function of the rear axle forces and the steady-state triplet $(R^{\rm ss}, V^{\rm ss}, \beta^{\rm ss})$:

$$\begin{aligned} f_F^{\rm ss} &= \sqrt{(f_{Fx}^{\rm ss})^2 + (f_{Fy}^{\rm ss})^2} \\ &= \sqrt{\frac{m^2(V^{\rm ss})^4}{(R^{\rm ss})^2} + (f_{Rx}^{\rm ss})^2 + (f_{Ry}^{\rm ss})^2 + 2\frac{m(V^{\rm ss})^2}{R^{\rm ss}}\left(f_{Rx}^{\rm ss}\sin\beta^{\rm ss} - f_{Ry}^{\rm ss}\cos\beta^{\rm ss}\right)}. \end{aligned}$$

Given the front axle normal load from (16), we also get

$$\mu_F^{\rm ss} = \frac{f_F^{\rm ss}}{f_{Fz}^{\rm ss}}, \qquad s_F^{\rm ss} = \mathrm{MF}^{-1}(\mu_F^{\rm ss}) = \tan\left(\mathrm{asin}(\mu_F^{\rm ss}/D)/C\right)/B.$$

Applying the friction circle equation (6) and the friction coefficient definition (5) at the front axle forces in equation (11) results in:

$$\frac{m(V^{\rm ss})^2}{R^{\rm ss}}\sin\beta^{\rm ss} = \frac{f_F^{\rm ss}}{s_F^{\rm ss}}(s_{Fx}^{\rm ss}\cos\delta^{\rm ss} - s_{Fy}^{\rm ss}\sin\delta^{\rm ss}) - f_{Rx}^{\rm ss}. \tag{21}$$

Recalling the definitions of front lateral slip and total front slip

$$\frac{s_{Fy}^{\rm ss}}{1+s_{Fx}^{\rm ss}} = \frac{V^{\rm ss}\sin(\beta^{\rm ss}-\delta^{\rm ss}) + V^{\rm ss}\ell_F\cos\delta^{\rm ss}/R^{\rm ss}}{V^{\rm ss}\cos(\beta^{\rm ss}-\delta^{\rm ss}) + V^{\rm ss}\ell_F\sin\delta^{\rm ss}/R^{\rm ss}} \tag{22}$$

$$s_F^{\rm ss} = \sqrt{(s_{Fx}^{\rm ss})^2 + (s_{Fy}^{\rm ss})^2}. \tag{23}$$

and solving equations (21), (22) and (23) for the front tire slip quantities and steering angle, leads finally to the computation of the longitudinal and lateral friction forces at the front wheel:

$$f_{Fj}^{\rm ss} = -\frac{s_{Fj}^{\rm ss}}{s_F^{\rm ss}}\mathrm{MF}(s_F^{\rm ss})f_{Fz}^{\rm ss}, \qquad j = x, y.$$

3.3 Steady-State Wheel Speeds and Torque Inputs

In Sections 3.1 and 3.2 we calculated the front and rear tire forces $f_{ij}^{\rm ss}$, $(i = F, R,\ j = x, y, z)$, the associated tire slip quantities $s_{ij}^{\rm ss}$, $(i = F, R,\ j = x, y)$ and the front wheel steering angle $\delta^{\rm ss}$ required to maintain a steady-state triplet $(R^{\rm ss}, V^{\rm ss}, \beta^{\rm ss})$. Next, we calculate the steady-state wheel speeds $\omega_i^{\rm ss}$, $(i = F, R)$ and input wheel torques $T_i^{\rm ss}$, $(i = F, R)$.

From the definition of the longitudinal wheel slip we find:

$$\omega_F = \frac{V_{Fx}}{(1+s_{Fx})r} = \frac{V\cos(\beta-\delta) + \dot\psi\ell_F\sin\delta}{(1+s_{Fx})r}, \tag{24}$$

$$\omega_R = \frac{V_{Rx}}{(1+s_{Rx})r} = \frac{V\cos\beta}{(1+s_{Rx})r}. \tag{25}$$

Neglecting rolling resistances at the front and rear tires, the equation describing the rotation of the wheels is as follows:

$$I_{wi}\dot\omega_i = T_i - f_{ix}r_i, \qquad i = F, R, \tag{26}$$

where I_{wi} $(i = F, R)$ is the moment of inertia of each wheel about its axis of rotation, r_i $(i = F, R)$ is the radius of each wheel and T_i is the driving/braking torque applied at each wheel. In steady-state motion the wheel speeds maintain constant values as in (24) and (25), thus equation (26) can be used to calculate the steady-state torques at each wheel:

$$T_i^{\rm ss} = f_{ix}^{\rm ss}r_i, \qquad i = F, R.$$

3.4 Steady-State Conditions: Numerical Examples

In this section we present several cases of steady-state cornering under the assumption of independent front and rear wheel torque control. For a given steady-state triplet $(R^{\text{ss}}, V^{\text{ss}}, \beta^{\text{ss}})$, we seek for the steady-state slip quantities, steering angle and tire friction forces at the front and rear tires using the derivations of Sections 3.1 and 3.2. In addition, we calculate the steady-state wheel speeds and torque inputs using the derivations of Section 3.3, as well as the front and rear wheel slip angle $\alpha_i^{\text{ss}} = \tan^{-1}(V_{iy}^{\text{ss}}/V_{ix}^{\text{ss}})$, $i = F, R$. The parameters of the vehicle used for the calculations are given in Table 1.

In Table 2 we present a number of steady-state conditions including the values of steady-state steering angle, front and rear wheel torques, angular rates and slip angles. We observe that multiple steady-states corresponding to the same path radius and vehicle speed are possible, as revealed by Cases (a) and (b), (k) and (n), (l) and (o), (m) and (p) in Table 2. At this stage we have assumed independent torque inputs for front and rear wheels. If we were to consider more traditional types of transmission, such as front-, rear-, and all-wheel-drive (FWD, RWD and AWD) we would need to classify these steady-states according to their feasibility with respect to a specific type of transmission. For instance, we notice that for the steady-state conditions (d), (g) and (j) the input torques satisfy $T_F^{\text{ss}} > 0$ and $T_R^{\text{ss}} > 0$, which are not achievable by a FWD or a RWD vehicle. The above steady-states require both front and rear powered wheels (AWD) with appropriate torque distribution. On the other hand for the steady-state conditions (a), (b), (f), (i), (k)-(p) the input torques satisfy $T_F^{\text{ss}} < 0$ and $T_R^{\text{ss}} > 0$, which are not achievable by a FWD vehicle. Finally, in Cases (c), (e) and (h) we observe that $T_F^{\text{ss}} > 0$ and $T_R^{\text{ss}} < 0$, which are not achievable by a RWD vehicle. The latter steady-states require front powered wheel (FWD or AWD) and rear braking torque, for instance by application of the handbrake, similar to expert race driving techniques. This classification of the steady-state equilibria according to the require wheel torques will be considered rigorously in future extensions of this work.

Traditional stability analysis techniques using the understeering gradient [Gillespie, 1992], assume high values of the corner radius R^{ss}, small values of sideslip β^{ss} and operation of the tires within their linear region. Hence, such techniques are not applicable to the operating regimes described in Table 2. For the given set of Magic Formula parameters in Table 1 it can be found that the maximum cornering tire force (assuming free rolling of the tire) is achieved at a slip angle of 11.9 deg. We notice that for all the cases of steady-state conditions listed, the rear tire has exceeded the saturation limit, operating well within the nonlinear region, as opposed to the front tire, which suggests oversteering behavior of the vehicle. In conditions (k), (l), (m), corresponding to the same cornering radius and slip angle, we observe that increasing steady-state velocity requires reduction of the steering angle (oversteering behavior). On the other hand, in conditions (n), (o), (p), corresponding to the same cornering radius and a common high value of sideslip, we have the opposite effect, that is, increasing speed requires an increase in the steering angle. However, we notice that in the cases (n), (o), (p), the high sideslip angle steady-states are achieved with steering angle opposite to the direction of the corner (counter-steering). The decrease of the amount of counter-steering with the increase in velocity at high sideslip angles has been noted in [Edelmann et al., 2008] for a steady-state cornering condition referred to as power-slide. While traditional stability analysis, such as in [Gillespie, 1992], is not applicable in the operating regimes studied in this work, stability analysis of drifting steady-state cornering conditions using phase-plane techniques appears in [Ono et al., 1998] and [Hindiyeh and Gerdes, 2009], or via root-locus in [Edelmann et al., 2008].

Table 1: *Vehicle Parameters.*

Parameter	**Value**
m (kg)	1450
I_z (kg m^2)	2741.9
ℓ_F (m)	1.1
ℓ_R (m)	1.59
h (m)	0.4
$I_{wF},\ I_{wR}$ (kgm^2)	1.8
$r_F,\ r_R$ (m)	0.3
B	7
C	1.6
D	1.0

Table 2: *Steady-state cornering conditions and associated torque and steering inputs.*

Case	R^{ss} (m)	V^{ss} (m/s)	β^{ss} (deg)	T_F^{ss} (Nm)	T_R^{ss} (Nm)	δ^{ss} (deg)	ω_F^{ss} (rad/s)	ω_R^{ss} (rad/s)	α_F^{ss} (deg)	α_R^{ss} (deg)
(a)	7	7	-10.4	-543	1194	3.2	22.27	32.08	-4.5	-22.5
(b)	7	7	-51	-56	1471	-40.7	20.44	58.33	-3.9	-57.9
(c)	7	6.12	-29	1649	-859	-13.7	21.13	2.9	-6.9	-39.1
(d)	7	7.41	-51	129	1456	-39.2	21.8	56.35	-5.4	-57.9
(e)	15	8.65	-33	1546	-902	-21.5	30.66	1.49	-7.8	-37.8
(f)	15	9.45	-29	-619	1375	-22.42	29.54	54.91	-2.9	-34
(g)	15	10.95	-51	38	1469	-42.53	34.25	75.45	-5.7	-54.5
(h)	1.5	3.42	-19	2031	-181	27.78	13.38	8.59	-4.4	-55.7
(i)	1.5	2.52	-37	-83	1376	11.36	6.76	38.37	-2	-64.3
(j)	1.5	3.42	-43	1267	1258	8.27	8.91	32.8	-4.2	-67.2
(k)	7	4	-6	-1395	1481	1.88	12.54	29.31	1.2	-18.4
(l)	7	5	-6	-1332	1478	1.1	15.69	29.36	2	-18.4
(m)	7	7	-6	-844	1213	-1.56	22.21	30.66	4.6	-18.4
(n)	7	4	-44	-845	1432	-37	11.56	69.35	0.2	-52
(o)	7	5	-44	-687	1450	-36	14.54	60.38	-0.7	-52
(p)	7	7	-44	-98	1400	-33	20.74	50.12	-3.9	-52

4 Stabilization of Cornering Equilibria

In the following we present a control scheme to stabilize the vehicle with respect to the previously derived steady-state conditions. The proposed control architecture consists of an LQR controller which provides the necessary front and rear wheel longitudinal slips (slip ratios) s_{Fx} and s_{Rx} to stabilize the vehicle to a specified steady-state triplet $(R^{ss}, V^{ss}, \beta^{ss})$. A sliding mode controller uses individual front and rear wheel torque inputs to drive the front and rear wheel longitudinal slips to the values specified by the LQR controller. We consider the steering angle δ as a parameter fixed to its steady-state value as calculated above, and we demonstrate stabilization of the system using purely longitudinal control. Vehicle handling using longitudinal control is used by expert rally drivers, who regulate throttle and brake inputs to stabilize a vehicle during cornering, by taking advantage of the longitudinal load transfer during acceleration and deceleration [Velenis et al., 2007a], [Velenis et al., 2007b], [Velenis et al., 2008a], [Velenis et al., 2008b].

4.1 Cornering Control Using Longitudinal Slip Inputs

We first express the equations of motion of the single-track model (1)-(3) in terms of the state variables V, β and $\dot{\psi}$:

$$\begin{aligned}
\frac{\mathrm{d}}{\mathrm{d}t}V &= f_1(V,\beta,\dot{\psi},s_{Fx},s_{Rx}) = \\
&= \frac{1}{m}\left[f_{Fx}\cos(\delta-\beta) - f_{Fy}\sin(\delta-\beta) + f_{Rx}\cos\beta + f_{Ry}\sin\beta\right] \qquad (27)\\
\frac{\mathrm{d}}{\mathrm{d}t}\beta &= f_2(V,\beta,\dot{\psi},s_{Fx},s_{Rx}) = \\
&= \frac{1}{mV}\left[f_{Fx}\sin(\delta-\beta) + f_{Fy}\cos(\delta-\beta) - f_{Rx}\sin\beta + f_{Ry}\cos\beta - mV\dot{\psi}\right] \qquad (28)\\
\frac{\mathrm{d}}{\mathrm{d}t}\dot{\psi} &= f_3(V,\beta,\dot{\psi},s_{Fx},s_{Rx}) = \\
&= \frac{\ell_F}{I_z}\left[f_{Fy}\cos\delta + f_{Fx}\sin\delta\right] - \frac{\ell_R}{I_z}f_{Ry}. \qquad (29)
\end{aligned}$$

The steady-state triplet $(R^{\mathrm{ss}}, V^{\mathrm{ss}}, \beta^{\mathrm{ss}})$ results in the equilibrium point $(V^{\mathrm{ss}}, \beta^{\mathrm{ss}}, \dot{\psi}^{\mathrm{ss}} = V^{\mathrm{ss}}/R^{\mathrm{ss}})$ of the above equations, that is

$$f_i(V^{\mathrm{ss}}, \beta^{\mathrm{ss}}, \dot{\psi}^{\mathrm{ss}}, s_{Fx}^{\mathrm{ss}}, s_{Rx}^{\mathrm{ss}}) = 0, \qquad i = 1,2,3,$$

where s_{ix}^{ss} $(i = F, R)$ are the steady-state front and rear wheel longitudinal slips, as calculated in Sections 3.1 and 3.2.

Equations (27)-(29) can be linearized as follows

$$\frac{\mathrm{d}}{\mathrm{d}t}\tilde{x} = \mathcal{A}^{\mathrm{ss}}\tilde{x} + \mathcal{B}^{\mathrm{ss}}\tilde{u}, \qquad (30)$$

where where $\mathcal{A}^{\mathrm{ss}}$ and $\mathcal{B}^{\mathrm{ss}}$ are the Jacobian matrices (with respect to the vehicle's state and slip inputs), computed at the equilibrium point $(V^{\mathrm{ss}}, \beta^{\mathrm{ss}}, \dot{\psi}^{\mathrm{ss}})$, and

$$\tilde{x} = \begin{bmatrix} V - V^{\mathrm{ss}} \\ \beta - \beta^{\mathrm{ss}} \\ \dot{\psi} - \dot{\psi}^{\mathrm{ss}} \end{bmatrix}, \quad \tilde{u} = \begin{bmatrix} s_{Fx} - s_{Fx}^{\mathrm{ss}} \\ s_{Rx} - s_{Rx}^{\mathrm{ss}} \end{bmatrix}, \quad \mathcal{C} = \mathcal{I}^{3\times 3}.$$

The eigenvalues of $\mathcal{A}^{\mathrm{ss}}$, which determine the stability of the equilibria are denoted by e_i, $i = 1,2,3$. An LQR state feedback control law $\tilde{u} = -\mathcal{K}\tilde{x}$ can then be readily computed using standard methods.

4.2 Stabilization of Steady-State Cornering via Sliding-Mode Control

In this section we design a sliding-mode control scheme to stabilize the vehicle with respect to steady-state equilibria incorporating the wheel angular rate dynamics, and using independent front and rear wheel torque control.

Consider the system (27)-(29) complemented by the dynamics of the rotating front and rear wheels (26). Recall that for a given operating condition of the vehicle $(V, \beta, \dot{\psi})$, a reference pair of front and rear longitudinal slip quantities s_{Fx} and s_{Rx} correspond to reference front and rear wheel speeds ω_F and ω_R, as in (24) and (25), respectively.

We define the variable $\tilde{z}_i$ as the difference between the actual wheel angular rate ω_i and a reference wheel angular rate corresponding to a reference value of longitudinal slip s_{ix}:

$$\tilde{z}_i = \omega_i - \phi_i(V,\beta,\dot{\psi}), \qquad i = F, R,$$

where

$$\phi_i(V,\beta,\dot{\psi}) = \frac{V_{ix}}{(1+s_{ix})r}, \qquad i = F, R.$$

The reference slip quantities s_{ix} in the expression above are generated by the LQR stabilizing control law.

Equation (31) results in

$$\begin{aligned} \dot{\tilde{z}}_i &= \frac{1}{I_w}T_i - \frac{r}{I_w}f_{ix} - \frac{\partial\phi_i}{\partial V}(V,\beta,\dot{\psi})f_1(V,\beta,\dot{\psi}) \\ &- \frac{\partial\phi_i}{\partial\beta}(V,\beta,\dot{\psi})f_2(V,\beta,\dot{\psi}) - \frac{\partial\phi_i}{\partial\dot{\psi}}(V,\beta,\dot{\psi})f_3(V,\beta,\dot{\psi}). \end{aligned} \tag{31}$$

Consider the control input

$$T_i = T_i^{\text{eq}} + I_w\hat{v}_i, \tag{32}$$

where

$$T_i^{\text{eq}} = f_{ix}r + I_w\left(\frac{\partial\phi_i}{\partial V}f_1 + \frac{\partial\phi_i}{\partial\beta}f_2 + \frac{\partial\phi_i}{\partial\dot{\psi}}f_3\right), \qquad i = F, R. \tag{33}$$

The control component T_i^{eq} is referred to as the *equivalent control*. Taking $T_i = T_i^{\text{eq}}$ results in $\dot{\tilde{z}}_i = 0$ and ensures that the vehicle's states will remain in the *sliding manifold* $\tilde{z}_i = 0$. Equations (31), (32) and (33) yield

$$\dot{\tilde{z}}_i = \hat{v}_i, \qquad i = F, R. \tag{34}$$

Finally, we take

$$\hat{v}_i = -\lambda_i \text{sat}(\tilde{z}_i), \quad \lambda_i > 0, \qquad i = F, R, \tag{35}$$

with

$$\text{sat}(\tilde{z}_i) = \begin{cases} \tilde{z}_i, & \text{if } |\tilde{z}_i| \leq 1, \\ \\ \text{sign}(\tilde{z}_i), & \text{if } |\tilde{z}_i| > 1. \end{cases}$$

It can be readily shown that the control (35) stabilizes (34) [Khalil, 1996]. In fact, all trajectories starting off the *sliding manifold* $\tilde{z}_i = 0$ will reach it in finite time under the control input (32). A schematic of the proposed control architecture is shown in Fig. 2.

4.3 Stabilization of Cornering Equilibria: Numerical Examples

We consider two simulation scenarios corresponding to Cases I and II of Table 3, where the stabilizing control law of the previous section is implemented. Both cases correspond to unstable equilibria along the same path radius, negotiated at the same speed. Case I is a steady-state condition of moderate vehicle slip angle, while Case II is one of excessive slip angle. With these scenarios we demonstrate the ability of the control scheme to stabilize a variety of equilibria, including aggressive cases (Case II), which resemble vehicle operating regimes met by expert rally-race drivers [Velenis et al., 2007a], [Velenis et al., 2007b], [Velenis et al., 2008a], [Velenis et al., 2008b].

The parameters of the vehicle model are shown in Table 1. In Case I, the simulation starts with initial states perturbed as follows,

$$V(0) = 1.2 \times V^{\text{ss}}, \quad \beta(0) = 2 \times \beta^{\text{ss}}, \quad \dot{\psi}(0) = 1.2 \times \dot{\psi}^{\text{ss}}, \tag{36}$$

Table 3: *Steady-State Cornering Equilibria.*

	Case I	Case II
$R^{\rm ss}$(m)	7	7
$V^{\rm ss}$(m/sec)	7	7
$\beta^{\rm ss}$(deg)	-10.4	-51
$s_{Rx}^{\rm ss}$	-0.2871	-0.7491
$s_{Fx}^{\rm ss}$	0.0244	0.0026
$\delta^{\rm ss}$(deg)	3.2	-40.7
e_1	0.7484 + 1.1395i	0.5790+0.7196i
e_2	0.7484 - 1.1395i	0.5790 -0.7196i
e_3	-9.9095	-8.8562

whereas in Case II the simulation starts from the following initial conditions:

$$V(0) = 1.2 \times V^{\rm ss}, \quad \beta(0) = \beta^{\rm ss}/2, \quad \dot{\psi}(0) = 1.2 \times \dot{\psi}^{\rm ss}. \tag{37}$$

In addition, we consider initial wheel speeds $\omega_F(0)$ and $\omega_R(0)$, such that the initial longitudinal slip at the front and rear wheels are both zero (free rolling wheels). The controller (32) is implemented in both cases with $\lambda_i = 100\,\sec^{-1}$, $(i = F, R)$.

The resulting trajectories for the two simulation scenarios are shown in Fig. 3. The vehicle states, torque control inputs and longitudinal wheel slips for the simulation Cases I and II are shown in Figs. 4 and 5, respectively. In the velocity V, sideslip angle β, yaw rate $\mathrm{d}\psi/\mathrm{d}t$ and longitudinal slips s_{ix} plots we present, in addition, the response of the vehicle model under the action of the LQR controller of section 4.1 (dotted curves) assuming longitudinal slip control inputs during stabilization from the same initial conditions. The wheel angular rates ω_F and ω_R corresponding to the response of the model under longitudinal slip inputs (dotted ω_F and ω_R curves) were calculated using equations (24) and (25), where s_{Fx} and s_{Rx} were the control inputs of the LQR controller. Hence, the dotted ω_i response curves correspond to the sliding manifold which is successfully met by the sliding mode controller T_i in finite time, in both Cases I and II.

In the design of the control scheme to stabilize the vehicle with respect to the steady-state cornering equilibria we have assumed exact knowledge of the tire/road friction forces via Pacejka's Magic Formula. In reality, such information is rarely accurately available due to the number of parameters that affect the tire-road interaction forces. To this end, we simulate the performance of the stabilizing controller in the presence of uncertainty in the tire friction. In particular, we assume uncertainty in the parameter D of the Magic Formula (6), which coincides with the maximum value of the friction coefficient for a given road condition. Typically $D = 0.9 - 1$ corresponds to dry asphalt surface, $D = 0.7 - 0.8$ corresponds to wet asphalt, $D = 0.5 - 0.6$ to gravel, and $D = 0.2$ to ice. In Figure 6 we present the vehicle response and torque control inputs during stabilization of the steady-state condition of Case II, where the controller is designed using a nominal value of $D = 1$, and tested in three different actual values of D, namely, $D = 1$, $D = 0.75$ and $D = 0.5$. We observe that the controller is successful in stabilizing the vehicle at a steady-state cornering condition. In the presence of uncertainty in the tire friction coefficient (cases of $D = 0.75$, $D = 0.5$) we notice a steady-state error in all of the vehicle states, and the error increases with the increase in the deviation of the friction coefficient. In particular, we observe that the vehicle is stabilized at a lower velocity and lower yaw rate than the initial steady-state condition of Case II, which is the result of the decrease in the friction coefficient and hence the maximum available cornering acceleration. We conclude that the control scheme introduces a level of robustness

with respect to the tire friction uncertainty, however, in order to avoid significant steady-state errors in the vehicle response, actual implementation of the controller will require real time tire friction estimation as demonstrated, for instance, in [Hsu and Gerdes, 2005] and [Piyabongkarn et al., 2009].

4.4 Incorporating Suspension Dynamics

In this section we implement the sliding mode controller using a vehicle model of increased fidelity. In particular, we introduce a single-track model with suspension dynamics, and demonstrate the performance of the controller in the same simulation scenarios as in the previous section.

Let z be the vertical displacement of the center of gravity of the vehicle and θ the pitch angle of the suspended mass as in Figure 7. The dynamics of the vertical translation and pitch rotation motions of the suspended mass are described by the following equations

$$m\ddot{z} = f_{Fz} + f_{Rz} - mg, \tag{38}$$

$$I_y\ddot{\theta} = f_{Rz}\ell_R\cos\theta - f_{Fz}\ell_F\cos\theta - \Sigma f_{Rx}\big(h+z\big) - \Sigma f_{Fx}\big(h+z\big), \tag{39}$$

where I_y is the moment of inertia of the vehicle about the y body axis, h is the vertical distance of the C.G. from the ground in an equilibrium state with $z = 0$, and Σf_{ix} $(i = F, R)$ is the projection of the total friction force of each wheel on the x body axis. Furthermore,

$$\Sigma f_{Rx} = f_{Rx} \quad \text{and} \quad \Sigma f_{Fx} = f_{Fx}\cos\delta - f_{Fy}\sin\delta$$

Given the vertical displacement of the C.G. z, and the pitch angle θ, the normal load of each wheel is given by

$$\begin{aligned} f_{Fz} &= f^o_{Fz} - K_F\Delta z_F - C_F\Delta\dot{z}_F \\ f_{Rz} &= f^o_{Rz} - K_R\Delta z_R - C_R\Delta\dot{z}_R \end{aligned}$$

where

$$\begin{aligned} \Delta z_R = z + \ell_R\sin\theta \quad &, \quad \Delta z_F = z - \ell_F\sin\theta \\ \Delta\dot{z}_R = \dot{z} + \dot{\theta}\ell_R\cos\theta \quad &, \quad \Delta\dot{z}_F = \dot{z} - \dot{\theta}\ell_F\cos\theta \end{aligned}$$

and

$$f^o_{Fz} = mg\frac{\ell_R}{\ell_F+\ell_R}\,, \qquad f^o_{Rz} = mg\frac{\ell_F}{\ell_F+\ell_R}.$$

Next, we present simulation results of the implementation of the sliding mode control law of Section 4.2 using the single-track model with suspension dynamics (27)-(29), (26), (38) and (39). The parameters of the vehicle model used are shown in Table 1. In addition, we use $K_F = K_R = 10000\,\text{N/m}$, $C_F = C_R = 2000\,\text{Nsec/m}$ and $I_y = 2741.9\,\text{kgm}^2$.

We consider two simulation scenarios of stabilizing the vehicle with respect to the equilibrium Cases I and II as in Table 3. The initial conditions in Cases I and II are given by (36) and (37) respectively. In addition, we consider initial wheel speeds $\omega_F(0)$ and $\omega_R(0)$ such that the initial longitudinal slip at the front and rear wheels are both zero, i.e. we enforce initial free rolling of the front and rear wheels. Finally, we assume zero initial vertical displacement and velocity and zero pitch angle and pitch rate ($z(0) = \dot{z}(0) = 0$, $\theta(0) = \dot{\theta}(0) = 0$). The controller (32) is implemented in both cases with $\lambda_i = 100\,\text{sec}^{-1}$, $(i = F, R)$. The resulting trajectories for the two simulation scenarios are shown in Fig. 8. The vehicle states, including the suspension dynamics states, and control inputs for the simulation Cases I and II are shown

in Figs. 9 and 10 respectively. The wheel torque control inputs and vehicle states corresponding to the sliding mode stabilization of the single-track model (27)-(29), (26) incorporating the static map of longitudinal acceleration to normal load transfer (9), (10) (neglecting the suspension dynamics) are also presented in Figs. 9 and 10 (dotted curves) for comparison. The sliding mode controller successfully stabilizes the higher order vehicle model including suspension dynamics, despite the fact that the steady-state cornering conditions were derived using the lower order vehicle model.

5 Conclusions

In this work we studied the control of wheeled vehicles in extreme operating conditions. We explicitly derived steady-state cornering conditions for a vehicle with the tires operating in their nonlinear region. The resulting trajectories included cases of aggressive sideslip angle similar to driving techniques used by expert rally drivers. Motivated by recently studied race driving techniques, we demonstrated that stabilization of these extreme steady-states may be achieved using longitudinal (accelerating/braking) control. In particular, we designed a sliding mode controller using front and rear wheel torque inputs to stabilize the vehicle dynamics with respect to the above steady-state cornering conditions. The controller's performance was validated by increasing the level of detail of the initial vehicle model to include suspension dynamics.

Plans for future work include the extension of the current results using vehicle models of increasing fidelity (e.g., four wheel models incorporating lateral load transfer effects) and implementation of the control scheme on an autonomous vehicle platform.

References

M. Abdulrahim. On the dynamics of automobile drifting. In *SAE World Congress*, Detroit, MI, April 3-6 2006.

J. Ackermann. Robust control prevents car skidding. *IEEE Control Systems Magazine*, 17: 23–31, 1997.

E. Bakker, L. Nyborg, and H.B. Pacejka. Tyre modelling for use in vehicle dynamics studies, 1987. SAE Paper No. 870421.

N.J. Dang. Preliminary results analysing the effectiveness of electronic stability control ESC systems, September 2004. www.nhtsa.dot.gov/cars/rules/regrev/evaluate/809790.html.

J. Edelmann, M. Plöchl, P. Lugner, W. Mack, and A. Falkner. Investigations on the powerslide of automobiles. In *9th International Symposium of Advanced Vehicle Control (AVEC)*, Kobe, Japan, October 6-9 2008.

E. Frazzoli. Discussion on "Optimality Properties and Driver Input Parameterization for Trail-Braking Cornering". *European Journal of Control*, 14(4), July-August 2008.

E. Frazzoli, M.A. Dahleh, and E. Feron. Real-time motion planning for agile autonomous vehicles. *Journal of Guidance, Control and Dynamics*, 25(1):116–129, 2002.

E. Frazzoli, M.A. Dahleh, and E. Feron. Maneuver-based motion planning for nonlinear systems with symmetries. *IEEE Transactions on Robotics*, 21(6):1077–1091, 2005.

T.D. Gillespie. *Fundamentals of Vehicle Dynamics*. Society of Automotive Engineers SAE International, Warrendale PA USA, 1992.

A. Hac and M.O. Bodie. Improvements in vehicle handling through integrated control of chassis systems. *International Journal of Vehicle Design*, 29(1/2):23–50, 2002.

R.Y. Hindiyeh and J.C. Gerdes. Equilibrium analysis of drifting vehicles for control design. In *Proceedings of the ASME 2009 Dynamic Systems and Control Conference*, Hollywood, CA, USA, October 12-14 2009.

Y.H.J. Hsu and J.C. Gerdes. Stabilization of a steer-by-wire vehicle at the limits of handling using feedback linearization. In *ASME International Mechanical Engineering Congress and Exposition*, Orlando, FL, USA, November 5-11 2005.

Y. Ikushima and K. Sawase. A study on the effects of the active yaw moment control. In *SAE International Congress and Exposition*, Detroit, MI, February 27 - March 2 1995.

H.K. Khalil. *Nonlinear Systems, 2nd edition*. Prentice Hall, Upper Saddle River, New Jersey, 1996.

D. Kim, S. Hwang, and H. Kim. Vehicle stability enhancement of four-wheel-drive hybrid electric vehicle using rear motor control. *IEEE Transactions on Vehicular Technology*, 57 (2):727–735, March 2008.

E. Ono, S. Hosoe, H.D. Tuan, and S. Doi. Bifurcation in vehicle dynamics and robust front wheel steering control. *IEEE Transactions on Control Systems Technology*, 6(3):412–420, May 1998.

D. Piyabongkarn, J.Y. Lew, R. Rajamani, J.A. Grogg, and Q. Yuan. On the use of torque biasing systems for electronic stability control: Limitations and possibilities. *IEEE Transactions on Control Systems Technology*, 15(3):581–589, May 2007.

D. Piyabongkarn, R. Rajamani, J.A. Grogg, and J.Y. Lew. Development and experimental evaluation of a slip angle estimator for vehicle stability control. *IEEE Transactions on Control Systems Technology*, 17(1):78–88, January 2009.

A. T. van Zanten, R. Erhardt, and G. Landesfeind, K. Pfaff. Vehicle stabilization by the vehicle dynamics control system ESP. In *IFAC Mechatronic Systems*, pages 95–102, Darmstadt, Germany, 2000.

F. Tahami, R. Kazemi, and S. Farhanghi. A novel driver assist stability system for all-wheel-drive electric vehicles. *IEEE Transactions on Vehicular Technology*, 52(3):683–692, May 2003.

A. Trachtler. Integrated vehicle dynamics control using active brake steering and suspension systems. *International Journal of Vehicle Design*, 36(1):1–12, 2004.

E. Velenis, P. Tsiotras, and J. Lu. Modeling aggressive maneuvers on loose surfaces: The cases of trail-braking and pendulum-turn. In *Proceedings of the 2007 European Control Conference*, Kos, Greece, July 2-5 2007a.

E. Velenis, P. Tsiotras, and J. Lu. Modeling aggressive maneuvers on loose surfaces: Data analysis and input parameterization. In *Proceedings of the 2007 Mediterranean Conference on Control and Automation*, Athens, Greece, June 27-29 2007b.

E. Velenis, P. Tsiotras, and J. Lu. Trail-braking driver input parameterization for general corner geometry. In *Proceedings of the SAE Motorsports Engineering Conference*, Concord, NC, USA, December 2-4 2008a.

E. Velenis, P. Tsiotras, and J. Lu. Optimality properties and driver input parameterization for trail-braking cornering. *European Journal of Control*, 14(4):308–320, July-August 2008b.

J. Wei, Y. Zhuoping, and Z. Lijun. Integrated chassis control system for improving vehicle stability. In *Proceedings of the IEEE International Conference on Vehicular Electronics and Safety*, Shanghai, China, December 6-9 2006.

J. Yi and E.H. Tseng. Nonlinear stability analysis of vehicle lateral motion with a hybrid physical/dynamic tire/road friction model. In *Proceedings of the ASME 2009 Dynamic Systems and Control Conference*, Hollywood, CA, USA, October 12-14 2009.

K. Yoshimoto, H. Tanaka, and S. Kawakami. Proposal of driver assistance system for recovering vehicle stability from unstable states by automatic steering. In *Proceedings of the IEEE International Vehicle Electronics Conference*, Changchun, China, September 6-9 1999.

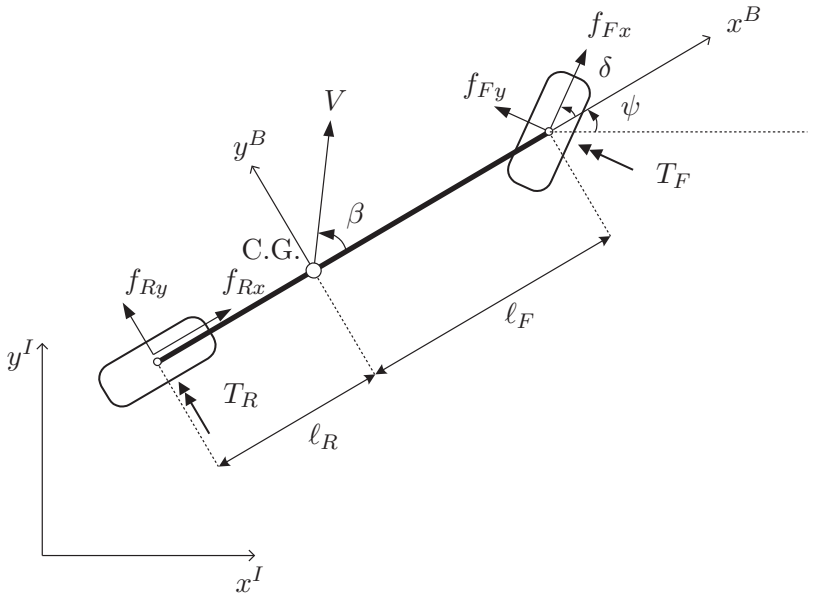

Figure 1: *Single-track vehicle model.*

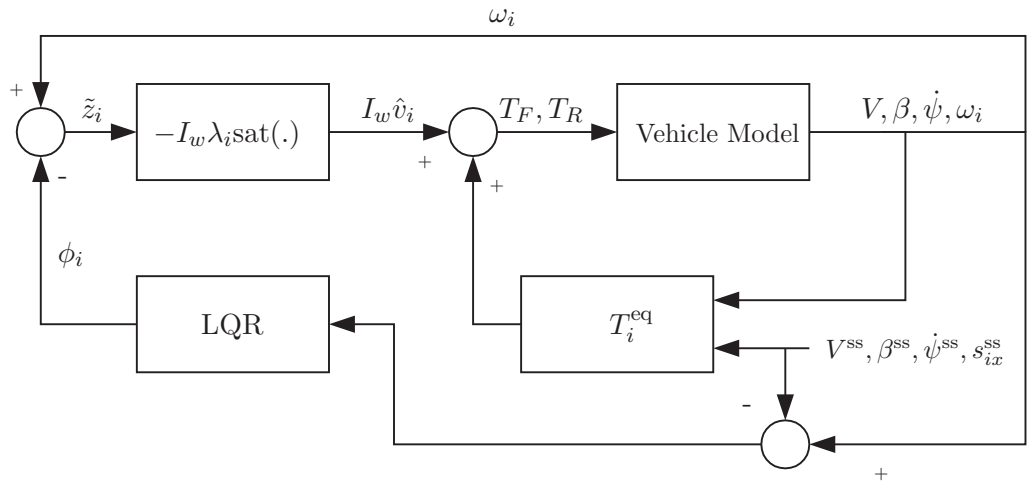

Figure 2: *Sliding mode control architecture for the stabilization of steady-state cornering conditions.*

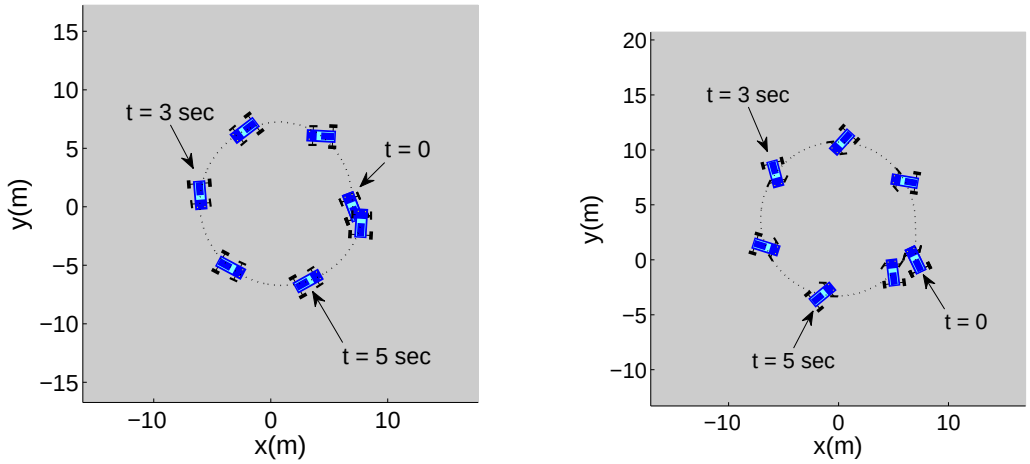

(a) (b)

Figure 3: *Steady-state cornering stabilization via sliding mode control; Simulation scenarios from Section 4.3: (a) Case I and (b) Case II.*

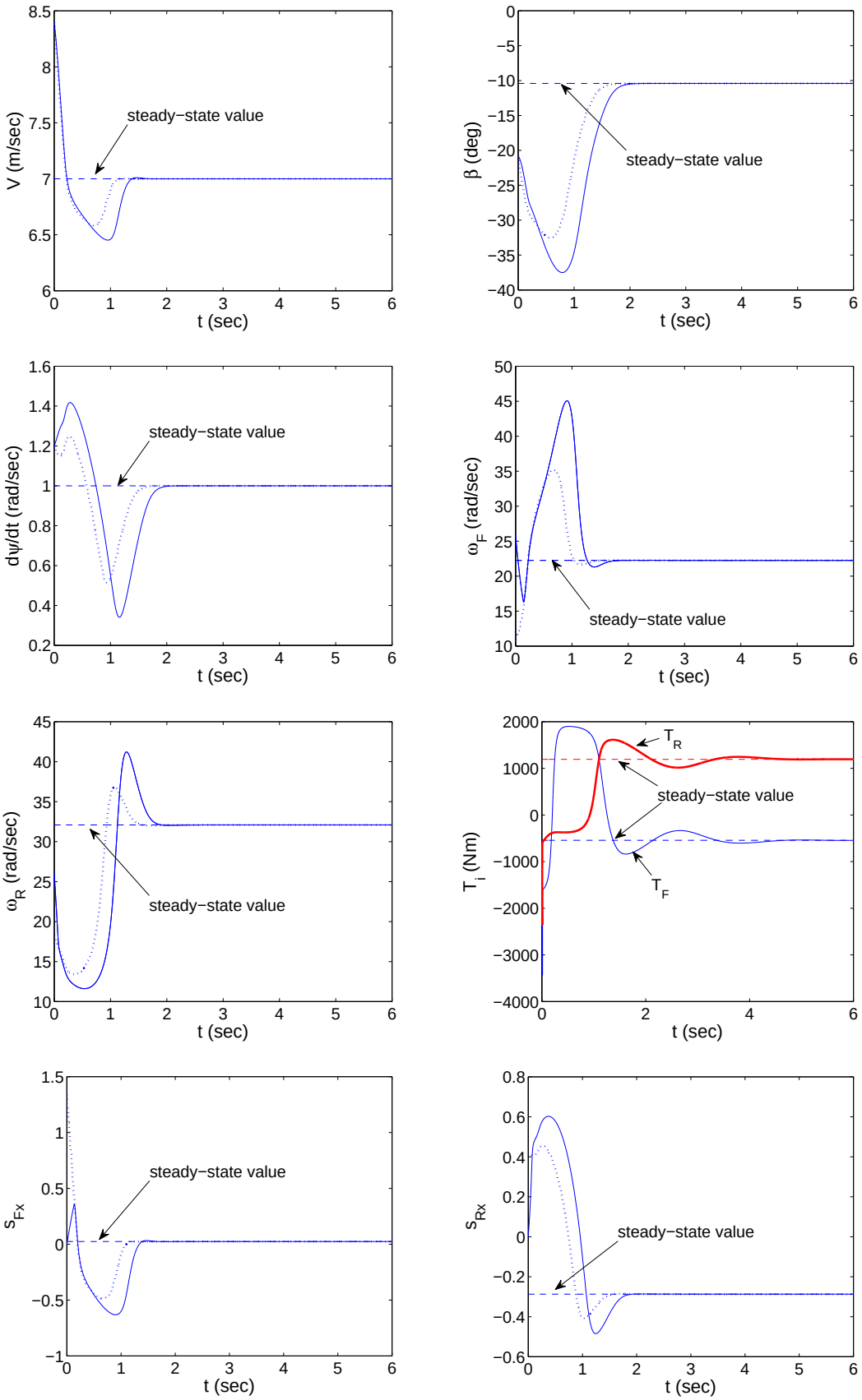

Figure 4: *Case I: Vehicle states, torque control inputs and longitudinal wheel slips. The dotted curves correspond to the stabilization of the vehicle model using longitudinal slip control inputs.*

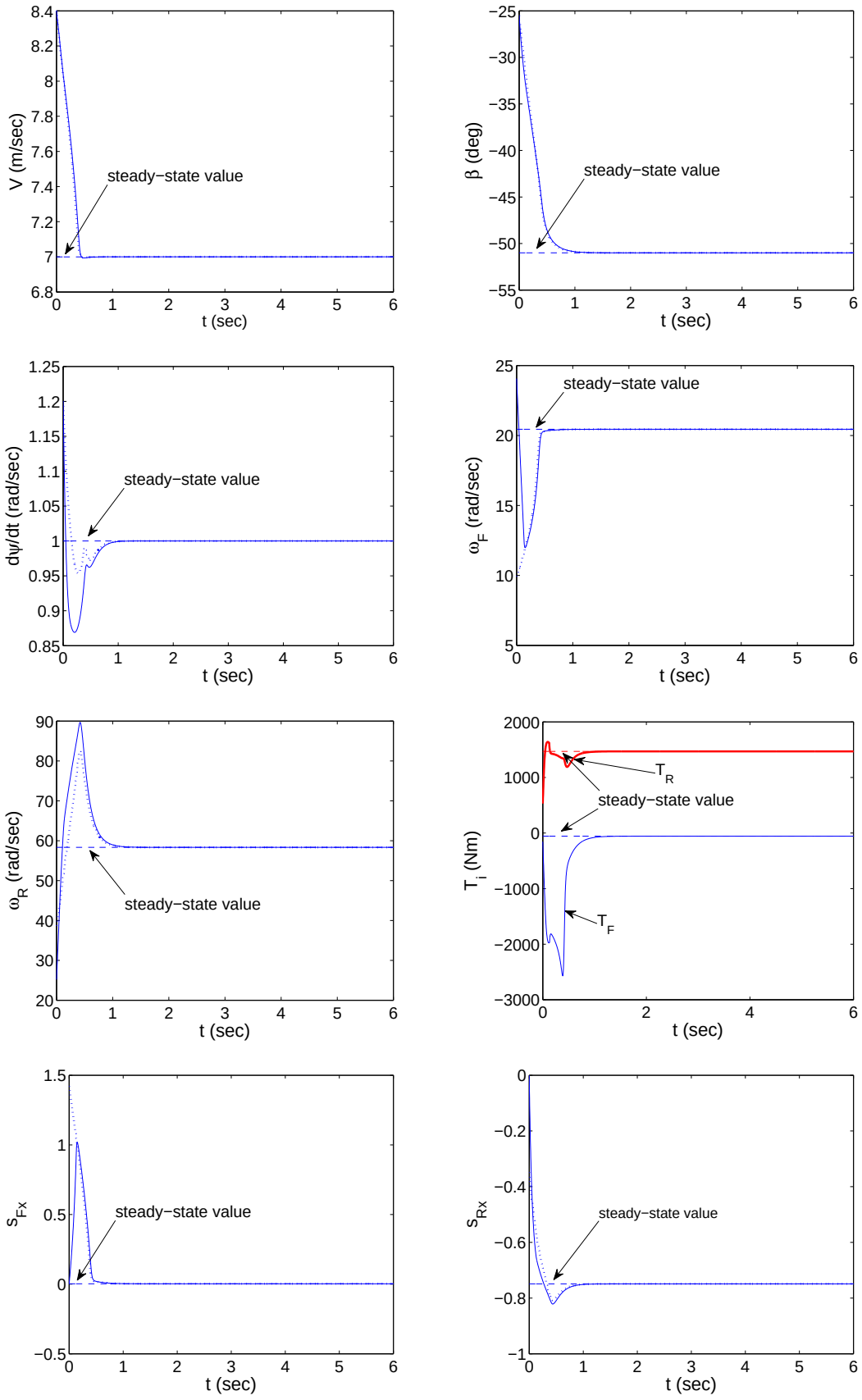

Figure 5: *Case II: Vehicle states, torque control inputs and longitudinal wheel slips. The dotted curves correspond to the stabilization of the vehicle model using longitudinal slip control inputs.*

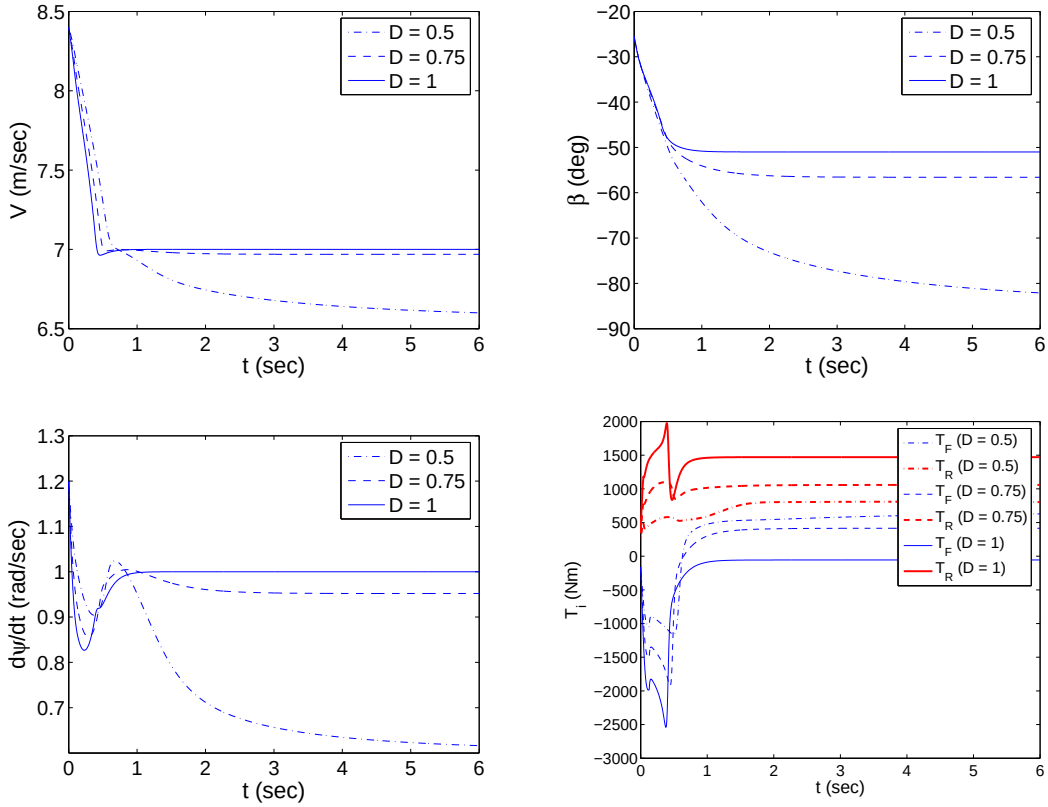

Figure 6: *Case II: Vehicle states and torque control inputs in the presence of tire friction uncertainty.*

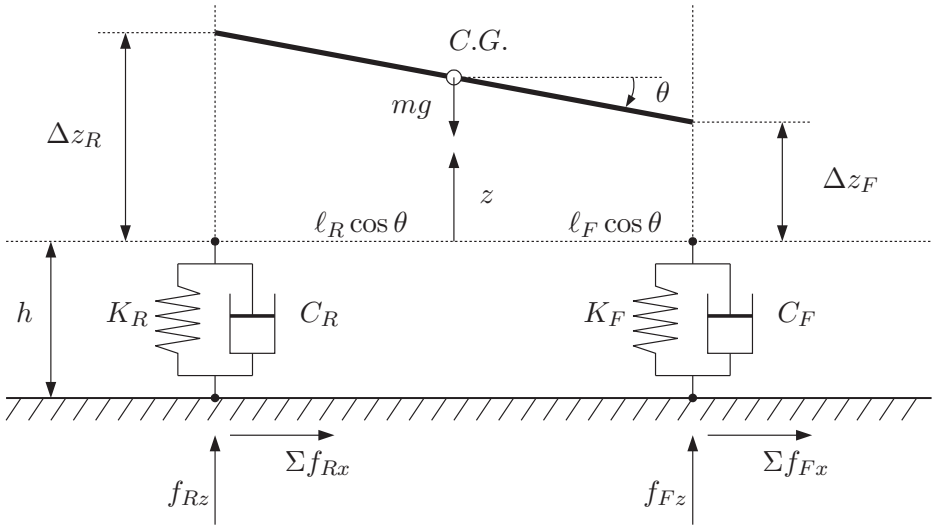

Figure 7: *Suspension Dynamics*

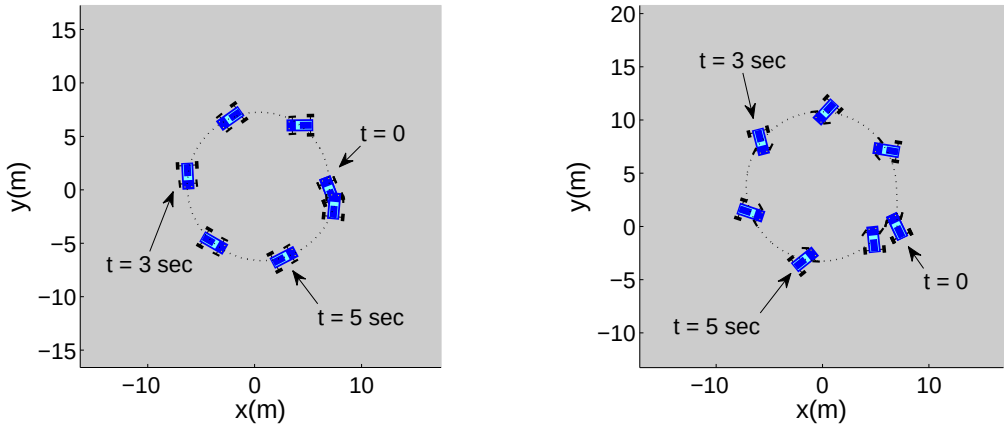

(a) (b)

Figure 8: *Steady-state cornering stabilization of a single-track model with suspension dynamics; Steady-state equilibrium points from Table 3 (a) Case I and (b) Case II.*

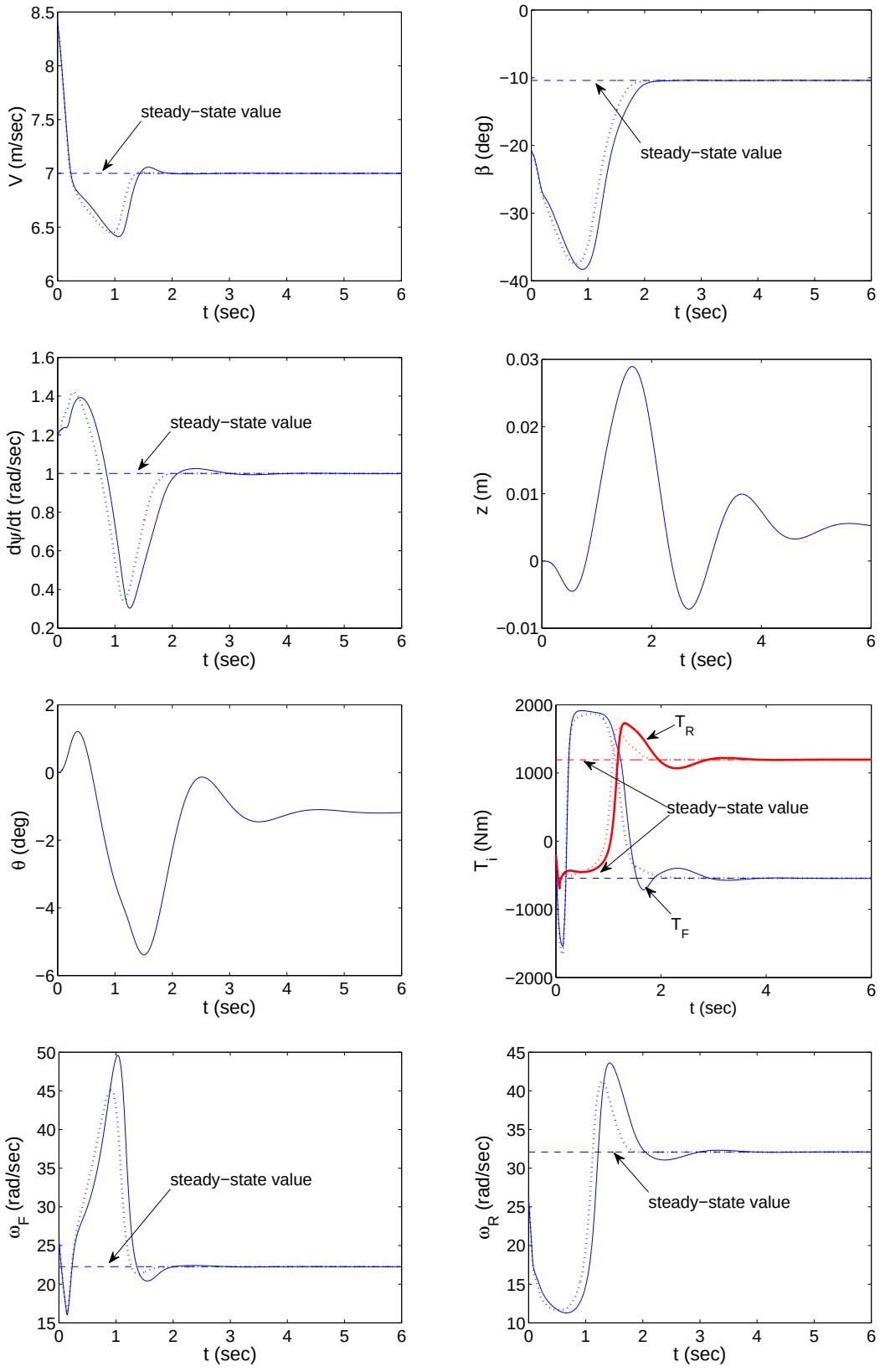

Figure 9: *Vehicle states and torque control inputs during stabilization of steady-state equilibrium point Case I. The dotted curves correspond to the stabilization of the vehicle model neglecting the suspension dynamics.*

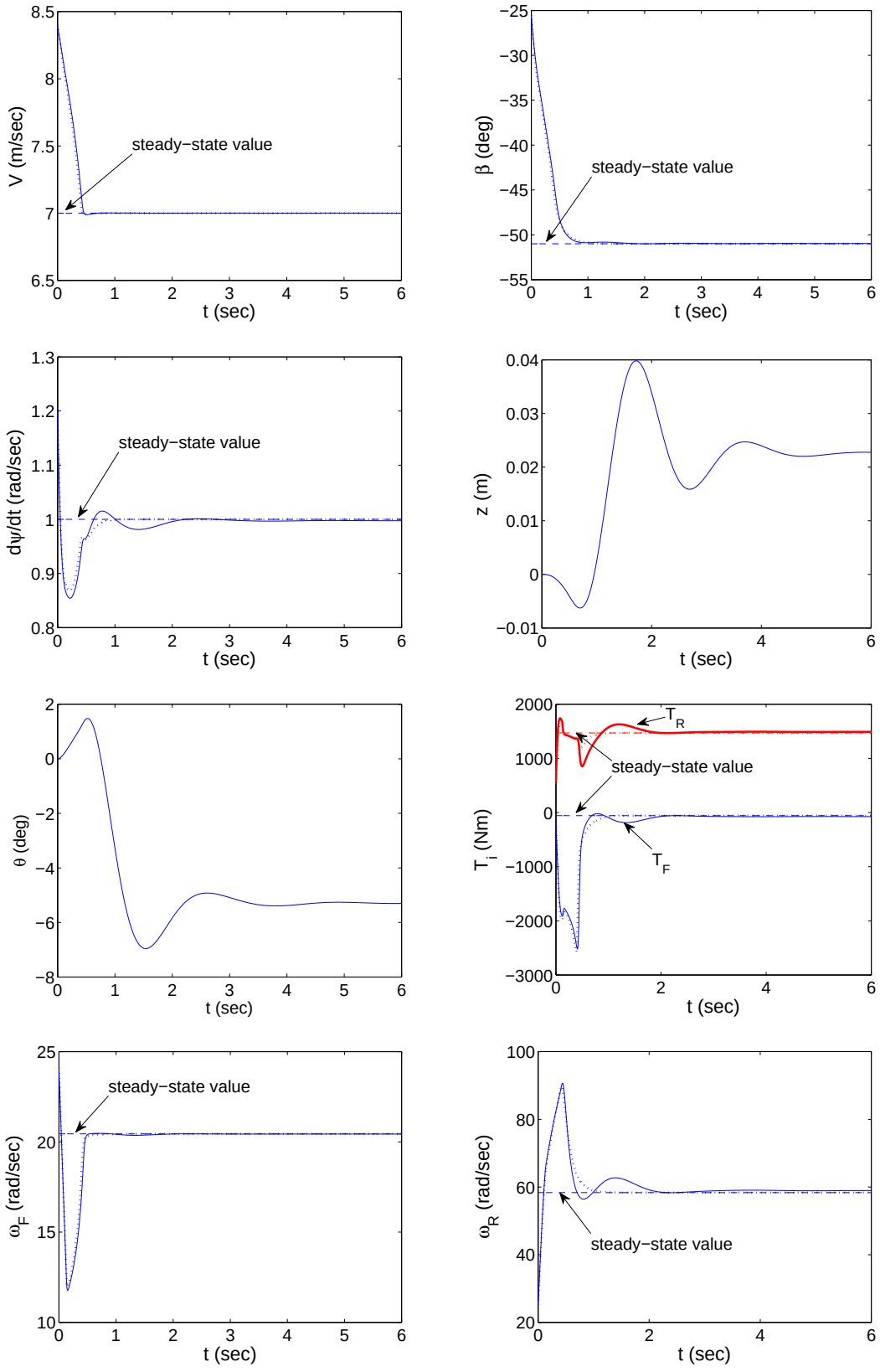

Figure 10: *Vehicle states and torque control inputs during stabilization of steady-state equilibrium point Case II. The dotted curves correspond to the stabilization of the vehicle model neglecting the suspension dynamics.*